



# A Beam Element Formulation for the Analysis of Isotropic and Anisotropic Thin-Walled Beams Using Cross Section Displacement Modes

*İnce Duvarlı Kirişlerin İzotropik ve Anizotropik Analizi İçin Kesit Değişim Modları Kullanılarak Bir Kiriş Elemanı Formülasyonu*

Yıldırım Serhat Erdoğan<sup>1</sup> , Mehmet Ada<sup>2\*</sup> 

<sup>1</sup>Yıldız Technical University, Faculty of Civil Engineering, Department of Civil Engineering, İstanbul, Türkiye

<sup>2</sup>Uşak University, Faculty of Engineering, Department of Civil Engineering, Uşak, Türkiye

## Abstract

This paper presents an efficient finite element (FE) formulation for the 3D linear static analysis of thin-walled beams through displacement modes obtained from cross-sectional analysis. The formulation is suitable for the analysis of cross-sections made of homogeneous isotropic and/or laminated composite materials with arbitrary shapes. The FE formulation concerns all the warping and the distortional effects arise from the non-uniform torsion and the shear/bending, which leads to a higher order beam element. Unlike similar approaches, the method does not require the determination of rigid modes and the utilization of a full modal matrix. Although the cross-section displacement modes obtained from the solution of a quadratic eigenvalue problem are generally complex, the formulation itself does not have to deal with calculations involving complex numbers. The numerical results presented comparatively for several cases, demonstrate the accuracy and the computational efficiency of the presented beam element formulation compared to solid and shell formulations.

**Keywords:** Cross-section displacement modes, cross-section distortion, laminated composite beams, thin-walled beams, warping effects.

## Öz

Bu makalede, kesit analizinden elde edilen yerdeğiştirme modları aracılığıyla ince cidarlı kirişlerin 3 boyutlu doğrusal statik analizini gerçekleştiren etkin bir sonlu elemanlar (SE) formülasyonu sunulmaktadır. Bu formülasyon, homojen izotropik ve/veya ince tabakalı kompozit malzemelerden yapılmış, gelişigüzel şekilli kesitlerin analizi için uygundur. Önerilen formülasyonda, kiriş elemanında yüksek dereceli etkiler oluşturan, düzensiz burulma ve kesme/eğilme kaynaklı tüm çarpılma ve şekil bozulma etkilerini dikkate alınmaktadır. Benzer yaklaşımlardan farklı olarak, bu yöntemde rijit modların belirlenmesi ya da bütün mod matrisinin kullanılmasına gerek bulunmamaktadır. İkinci dereceden özdeğer problemi çözümünden elde edilen kesit yer değiştirme modlarının genellikle karmaşık sayı olması rağmen, bu formülasyonda karmaşık sayılarla hesaplama yapılmasına da gerek yoktur. Birkaç durum için karşılaştırmalı olarak sunulan sayısal sonuçlar, sunulan kiriş elemanı formülasyonunun katı ve kabuk formülasyonlarına kıyasla doğruluğunu ve hesaplama verimliliğini göstermektedir.

**Anahtar Kelimeler:** İnce cidarlı kirişler, katmanlı kompozit kirişler, çarpılma etkileri, kesitsel bozulma, en kesit yerdeğiştirme modları.

\*Corresponding author: mehmet.ada@usak.edu.tr

Yıldırım Serhat Erdoğan  [orcid.org/0000-0001-9206-5474](https://orcid.org/0000-0001-9206-5474)

Mehmet Ada  [orcid.org/0000-0002-7099-590X](https://orcid.org/0000-0002-7099-590X)



## 1. Introduction

As it is well known, the role of beam elements is crucial in the analysis of structural systems encountered in many engineering fields such as civil, mechanical and aerospace engineering. Due to their computational efficiency, beam elements are commonly used in the design and analysis of complex structural and mechanical systems. Recently, with the developments of advanced and composite materials, the applications of high strength thin-walled elements in the engineering fields have substantially increased. However, the distinctive behavior of thin-walled sections due to the warping and the distortional effects does not enable the application of the classical Bernoulli and the Timoshenko beam theories in the deformation analysis. Hence, significant effort has been spent to improve the accuracy and the efficiency of the 1D beam elements to accurately predict the 3D stress and the deformation fields.

Since the Vlasov's theory (Vlasov 1961), which considers the additional stresses due to warping in the beam element formulation, many researches focused on including the warping effects in finite element (FE) formulations (Giavotto et al. 1983, Bauld and Tzeng 1984, Borri and Merlini 1986). However, the distortion of the cross-section was ignored in many formulations. With the evolution of the finite element method, displacement-based finite element formulations which takes into account the lateral-torsional stability problems of the thin-walled beams were formulated by Krajcinovic (1969), Barsoum and Gallagher (1970), Bažant and El Nimeri (1973). Erkmén and Mohareb (2006) developed a theory for the torsional analysis of open thin-walled beams. A shear-locking-free beam element for the analysis of coupled flexural and torsional effects of thin-walled closed sections beams was proposed by Wang et al. (2014). Stoykov et al. (2016) derived a 3D beam model based on Timoshenko theory considering that the cross-section rotates as a rigid body, yet, deforms longitudinally. Pavazza et al. (2022) introduced a novel theory for the torsion of bars based on Vlasov's theory and Timoshenko's beam theory for beams with open thin-walled sections. Although warping displacements are much smaller than 1D beam deformations, it is crucial to model warping accurately. This is because the stress field depends on the derivatives of warping, which can be large (Hodges 2006). Addessi et al. (2021) proposed three FE formulations, based on the enriched kinematics to account for the warpings and coupling between axial/bending and shear/torsion. A numerical procedure was followed to numerically calculate the warping functions.

Recently, Gabbianelli (2021) adopted a relatively new numerical method called the applied element method to simulate warping effects in typical steel rack members. One of the first attempts at the inclusion of in-plane distortions of thin-walled sections was made by Jönsson (1999). The study shows the differences in the governing torsional and distortional parameters between the open and closed sections. Recently, generalized beam theory (Davies and Leach 1994, Bianco et al. 2018) and refined beam theories (Carrera et al. 2011) have become popular since they enable all warping and distortional effects to be taken into consideration. These methods are basically based on finding warping modes by cross-sectional analysis. Vieira et al. (2014) presented a higher-order model for linear prismatic thin-walled beams, which includes out-of-plane and transversal section deformations. The displacement field was approximated by globally defined basis functions over the cross-section, and the uncoupled displacement modes were found by solving a nonlinear eigenvalue problem. A novel cross-section mode determination procedure, which leads to the 3D beam displacements mode was introduced by Hansen and Jönsson (2019a). Similarly, in Jönsson and Andreassen (2011) and Hansen and Jönsson (2019b), the walls of the beam sections were modeled by beam elements, and the nodal degrees of freedom were interpolated by standard beam shape functions. The calculated full complex displacement mode matrix was directly used in the FE formulation. However, their formulation requires the determination of rigid displacement modes, which is a rather complicated procedure. Ferradi and Cespedes (2014) used enriched kinematics to describe transversal deformations and warping by sectional analysis discretized by 1D and triangular elements. Jang et al. (2012) presented a study that investigates the static and eigenvalue analysis of thin-walled straight beams considering warpings and distortional deformations in addition to the standard Timoshenko displacement field. A more recent 3D finite element model with low computational cost for coupled bending and torsional-warping analysis of thin-walled beams was introduced by Lezgy-Nazargah et al. (2021). Liang et al. (2024) proposed a novel reduced-order method for geometrically nonlinear analysis of thin-walled structures with large deflections, developing mixed nonlinear kinematics using co-rotational and updated von Kármán formulations.

Meanwhile, the development of advanced composite materials has paved the way for the use of high strength thin-walled structural beams. Thus, many researchers developed

techniques to deal with the coupling deformations in addition to the warping and distortional effects in thin-walled laminated beams. The first attempts include the studies related to the application of shear deformable theories to account for the flexural-torsional response of thin-walled laminated composite beam analysis (Lee and Lee 2004, Lee 2005, Sheikh and Thomsen 2008, Vo and Lee 2008, Vo and Lee 2009, Vukasović et al. 2017). Afterwards, several attempts have been made to develop techniques for the analysis of thin-walled beams with arbitrary cross by separating 3D problems into 2D and 1D problems. Hence, 2D cross-section analyses have been used to obtain the cross-section stiffness matrix to be used in 1D beam element formulations. Although this approach dates back to the paper of Berdichevskii (1979), variational asymptotic beam sectional analysis (VABS) proposed in Clesnik and Hodges (1997), has been paid a lot of attention. The recent updates of this technique were discussed in Yu et al. (2012). A multifield variational sectional analysis method was introduced by Dhadwal and Jung (2019). They treated stresses and warping deformations as unknowns in their formulations. By introducing an analytical function for both primary and secondary warping, a kinematically exact rod model for thin-walled open-section members was proposed by Kassab et al. (2003). Prokić (1994) conducted an analysis of thin-walled beams with arbitrary open or closed cross-sections subjected to elasto-plastic deformations. The solution strategy was based on the finite-element method and incremental techniques, incorporating a novel model for cross-sectional warping that considers shear deformation effects. In Prokić (1996a) expanded Prokić (1994) by introducing a more general warping function, which improved upon the classical theory of thin-walled structures, where the cross-section is assumed to remain undeformed in its plane. The study utilized the principle of virtual displacements to establish the equilibrium condition, and the stresses were directly calculated from the corresponding strains. Additionally, Prokić (1996b) provided further details on the implementation of the proposed method. A new model has been developed by Vojnić-Purčar et al. (2019) to describe the shear lag in laminated composite thin-walled beams with openings, where warping of open-closed cross-sections is defined by displacement parameters at selected nodes based on the warping functions introduced by Prokić (1996a and 1996b). The finite element method is used for the solution, with a linear stiffness matrix derived from the principle of virtual displacements, and stresses are calculated directly from the strains without relying on Vlasov's assumption. Deo and

Yu (2020) used the mechanics of the structure genome approach to develop an efficient beam cross-sectional model with anisotropic materials in the FE framework. Recently, the work of Giavotto et al. (1983) was extended by Kashefi et al. (2016) and Islam et al. (2021) to develop a method, in which the cross-section stiffness matrix is obtained first and then utilized in 1D FE beam element formulation for global response analysis. Although their formulation seems generic, the method was not verified against non-uniform torsion. Osman et al. (2024) developed a family of 13 degree-of-freedom elements for analyzing the elastic buckling of thin-walled I-beams, incorporating the effects of web distortion. Shen (2024) modeled thin-walled beams using the absolute nodal coordinate formulation, capturing warping and distortion with Taylor-like polynomials. In this study, Linear Lagrange interpolation and cubic Hermite interpolation were used for the off-axis position vectors. Alongside the aforementioned methods, other approaches such as finite difference (Mottram 1992, Evseev and Morozov 1997, Soltani and Asgarian 2018), finite strip (Van Erp and Menken 1990, Yanlin and Shaofan 1991, Ádány and Schafer 2014, Naderian and Ronagh 2015, Liu et al. 2023), boundary element (Palermo et al. 1992, Zhang et al. 2011, Dikaros and Sapountzakis 2014) are also utilized to solve thin-walled beams.

This study presents a higher-order 3D beam FE formulation for the analysis of thin-walled members with arbitrary cross-sections made of isotropic or laminated composite materials. The 3D beam analysis is divided into 2D sectional analysis with quadrilateral elements and 1D beam FE analysis using linear or cubic interpolation functions. The section displacement modes are obtained by solving a quadratic eigenvalue problem and adopted as the warping and distortional displacement modes in the FE formulation. Hence, the in-plane and the out-of-plane distortions of the cross-section are efficiently concerned. In addition to the section displacements resulting from the rigid translations and the rotations, the constants of the displacement modes are taken as nodal degrees of freedom in the beam element formulations. Fortunately, only several numbers of modes were found to be enough for accurate predictions, which resulted in an efficient beam element. As distinct from its counterparts, the formulation does not require the full displacement mode matrix and does not have to deal with complex numbers resulting from the solution of the quadratic eigenvalue problem. Additionally, there is no need for complicated procedures to determine the fundamental

modes resulting from rigid body motions. The quadratic eigenvalue problem, which might be computationally expensive in the case of dense section discretization, especially for laminated composite materials, is linearized and solved for the first few smallest eigenvalues. Although the formulation uses the 3D constitutive material matrix, a reduced material matrix with plane stress/strain assumption can easily be adopted. Additionally, warping constraints can easily be introduced by constraining the displacement mode constants at the boundaries, and the determination of any shear, torsional and warping constants is not needed. A MATLAB code has been developed to implement the proposed FE model. The accuracy of the beam element derived from the present approach is verified by several numerical examples that exist in the literature.

## 2. Kinematics of the Higher Order Beam

The assumption is that the beam-like composite structure has a prismatic, slender geometry and exhibits no sudden variations in its cross-sectional shape or material properties. Gradual elastic deformations arise along the beam due to the applied loads. The kinematics of the beam are considered by taking the longitudinal (warping) and the transversal (distortional) deformation modes into account in the calculation of the 2D formulation. Thus, the deformations that can occur in the beam have been incorporated into the analysis. The conventional treatments and notions adopted in Islam et al. (2021) are followed and summarized for the completeness of the formulation.

The prismatic thin-walled beam member is located in a global rectangular, right-handed Cartesian coordinate system ( $X, Y, Z$ ). The cross-section of the beam situates in the  $X$ - $Y$  plane, and the beam axis is straight and parallel to the  $Z$  axis. The displacement vector  $\mathbf{u}(x, y, z)$  consists of three components in a material point on the cross-section is separated into rigid plane translations/rotations  $\mathbf{u}^r(x, y, z)$  and the warping/distortional components  $\mathbf{u}^d(x, y, z)$  as given in Eq. (1)

$$\mathbf{u} = \mathbf{u}^r + \mathbf{u}^d \quad (1)$$

where  $\mathbf{u}^r$  and  $\mathbf{u}^d$  can be expressed in terms of the section displacement vector  $\mathbf{U}(z) = \{U_x, U_y, U_z, \theta_x, \theta_y, \theta_z\}^T$  defined in the section centroid as

$$\begin{bmatrix} u_x^r \\ u_y^r \\ u_z^r \end{bmatrix} = \begin{bmatrix} 1 & 0 & 0 & 0 & 0 & -y \\ 0 & 1 & 0 & 0 & 0 & x \\ 0 & 0 & 1 & y & -x & 0 \end{bmatrix} \text{ or } \mathbf{u}^r = \mathbf{Z}\mathbf{U} \quad (2)$$

The cross-section is discretized in the FE sense, thus the distortional displacements can be interpolated over the cross-section using 2D quadrilateral elements in terms of shape functions and distortional displacements as

$$\mathbf{u}^d = \mathbf{N}_q \quad (3)$$

where  $\mathbf{N}$  is the shape function matrix of the 2D elements and  $\mathbf{q} = [q_x^1 q_y^1 q_z^1 q_x^2 q_y^2 q_z^2 \dots q_x^{nd} q_y^{nd} q_z^{nd}]^T$  consists of the nodal values of the distortional displacements in  $X, Y, Z$  directions (Figure 1). The size of  $\mathbf{q}$  and  $\mathbf{N}$  depends on the number of nodes  $nd$  in the FE discretization of cross-section.

The strain vector can be defined in terms of the displacement derivatives with those concerning the in-plane coordinates ( $x$  and  $y$ , the beam's sectional coordinates) separated from those corresponding to the out-of-plane coordinate ( $z$ , the beam's axial direction) as follows

$$\begin{aligned} \boldsymbol{\varepsilon} = \begin{Bmatrix} \varepsilon_x \\ \varepsilon_y \\ \gamma_{xy} \\ \gamma_{xz} \\ \gamma_{yz} \\ \varepsilon_z \end{Bmatrix} &= \begin{bmatrix} \frac{\partial}{\partial x} & 0 & 0 \\ 0 & \frac{\partial}{\partial y} & 0 \\ \frac{\partial}{\partial y} & \frac{\partial}{\partial x} & 0 \\ 0 & 0 & \frac{\partial}{\partial x} \\ 0 & 0 & \frac{\partial}{\partial y} \\ 0 & 0 & 0 \end{bmatrix} \begin{Bmatrix} u_x \\ u_y \\ u_z \end{Bmatrix} + \begin{bmatrix} 0 & 0 & 0 \\ 0 & 0 & 0 \\ 0 & 0 & 0 \\ 1 & 0 & 0 \\ 0 & 1 & 0 \\ 0 & 0 & 1 \end{bmatrix} \frac{\partial}{\partial z} \begin{Bmatrix} u_x \\ u_y \\ u_z \end{Bmatrix} \\ &= \partial_{xy} \mathbf{u} + s \mathbf{u}_{,z} \end{aligned} \quad (4)$$

Substitution of Eqs. (1), (2) and (3) into Eq. (4) yields to

$$\boldsymbol{\varepsilon} = \mathbf{S}\mathbf{Z}\mathbf{Y} + \mathbf{B}\mathbf{q} + \mathbf{S}\mathbf{N}\mathbf{q}_{,z} \quad (5)$$

where  $\mathbf{B} = \partial_{xy} \mathbf{N}$  and  $\mathbf{Y}$  is the sectional strain vector which comprises six strain components (two shear strains, axial strain, two curvatures, and torsional strain) assuming no distortion

$$\mathbf{Y} = \begin{Bmatrix} U_{x,z} - \theta_y \\ U_{y,z} + \theta_x \\ U_{z,z} \\ \theta_{x,z} \\ \theta_{y,z} \\ \theta_{z,z} \end{Bmatrix} = \begin{bmatrix} 0 & 0 & 0 & 0 & -1 & 0 \\ 0 & 0 & 0 & 1 & 0 & 0 \\ 0 & 0 & 0 & 0 & 0 & 0 \\ 0 & 0 & 0 & 0 & 0 & 0 \\ 0 & 0 & 0 & 0 & 0 & 0 \\ 0 & 0 & 0 & 0 & 0 & 0 \end{bmatrix} \begin{Bmatrix} U_x \\ U_y \\ U_z \\ \theta_x \\ \theta_y \\ \theta_z \end{Bmatrix} + \begin{Bmatrix} U_{x,z} \\ U_{y,z} \\ U_{z,z} \\ \theta_{x,z} \\ \theta_{y,z} \\ \theta_{z,z} \end{Bmatrix} \text{ or}$$

$$\mathbf{Y} = \mathbf{L}\mathbf{U} + \mathbf{U}_{,z} \quad (6)$$

In order to constitute the strain-stress relationship, the 3D linear elastic material matrix can be used for isotropic materials. However, the 3D orthotropic material matrix  $\mathbf{Q}$  of a lamina, which includes the six independent constants  $E_1, E_2, E_3, G_{12}, G_{13}, G_{23}, \nu_{12}, \nu_{13}$ , and  $\nu_{23}$  should be adopted for



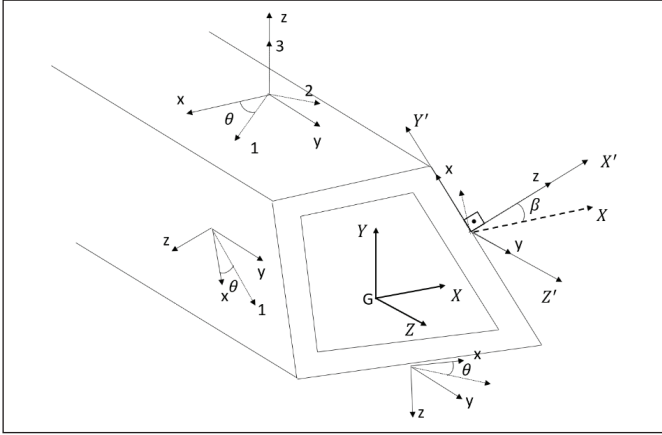


**Figure 1.** Representations of lamina-laminate configurations and beam coordinate system.

laminated composite materials as given in many textbooks (Reddy 2004, Barbero 2018). Additionally, coordinate transformations of the 3D material matrix are needed to account for the fiber and laminate orientation described in Figure 1. Hence, the constitutive relationship of a ply/lamina, defined in its material coordinate system, can be converted into the laminate coordinates by using the fiber orientation angle  $\theta$ , the laminate orientation angle  $\beta$ , and applying additional transformations. Thus, the constitutive relationship of a lamina can be obtained as

$$\boldsymbol{\varepsilon} = T_4 T_3 T_2 T_1 Q T_1^T T_2^T T_3^T T_4^T \quad (7)$$

where  $T_1$  is used to transform the material constitutive relationship from lamina coordinate system (1-2-3) to laminate coordinate system ( $x-y-z$ ),  $T_2$  transforms the coordinate system from ( $x-y-z$ ) to ( $X'-Y'-Z'$ ) and  $T_3$  transforms the coordinate system from ( $X'-Y'-Z'$ ) to ( $X-Y-Z$ ). Finally,  $T_4$  performs a transformation between  $\bar{\boldsymbol{\varepsilon}} = [\varepsilon_{xx}, \varepsilon_{yy}, \varepsilon_{zz}, \varepsilon_{yz}, \varepsilon_{xz}, \varepsilon_{xy}]$ ,  $\bar{\boldsymbol{\sigma}} = [\sigma_{xx}, \sigma_{yy}, \sigma_{zz}, \sigma_{yz}, \sigma_{xz}, \sigma_{xy}]$  and  $\boldsymbol{\varepsilon}, \boldsymbol{\sigma}$ .

$$T_1 = \begin{bmatrix} m^2 & n^2 & 0 & 0 & 0 & -2mn \\ n^2 & m^2 & 0 & 0 & 0 & 2mn \\ 0 & 0 & 1 & 0 & 0 & 0 \\ 0 & 0 & 0 & m & n & 0 \\ 0 & 0 & 0 & -n & m & 0 \\ mn & -mn & 0 & 0 & 0 & m^2 - n^2 \end{bmatrix} \quad (8)$$

$$T_2 = \begin{bmatrix} 0 & 0 & 1 & 0 & 0 & 0 \\ 1 & 0 & 0 & 0 & 0 & 0 \\ 0 & 1 & 0 & 0 & 0 & 0 \\ 0 & 0 & 0 & 0 & 0 & 1 \\ 0 & 0 & 0 & 1 & 0 & 0 \\ 0 & 0 & 0 & 0 & 1 & 0 \end{bmatrix} \quad (9)$$

$$T_4 = \begin{bmatrix} 1 & 0 & 0 & 0 & 0 & 0 \\ 0 & 1 & 0 & 0 & 0 & 0 \\ 0 & 0 & 0 & 0 & 0 & 1 \\ 0 & 0 & 0 & 0 & 1 & 0 \\ 0 & 0 & 0 & 1 & 0 & 0 \\ 0 & 0 & 1 & 0 & 0 & 0 \end{bmatrix} \quad (10)$$

where  $m = \cos \theta$ ,  $n = \sin \theta$ , and  $T_3$  is identical to  $T_1$  with  $\theta$  is replaced by  $\beta$ .

### 3. Calculation of the Cross-Section Displacements Modes

The process of determining the cross-section mode involves solving displacement mode differential equations by assuming exponential solutions. This is accomplished by solving the characteristic equations, which are formulated as a quadratic eigenvalue problem. Having accounted for the kinematic and constitutive relations, the linear elastic strain energy can be formulated as follows:

$$U_e = \frac{1}{2} \int_V \boldsymbol{\varepsilon}^T \boldsymbol{\sigma} dV = \frac{1}{2} \int_l \int_A \boldsymbol{\varepsilon}^T \boldsymbol{\sigma} dA dz \quad (11)$$

By substituting Eqs. (5), (6) and (7), the strain energy expression takes the following form

$$U_e = \frac{1}{2} \int_l \int_A [SZY + Bq + SNq_{,z}]^T Q [SZY + Bq + SNq_{,z}] dA dz \quad (12)$$

Taking the first variation of Eq. (12), the strain energy variation is obtained as

$$\delta U_e = \int_l \int_A \begin{Bmatrix} \delta Y \\ \delta q \\ \delta q_{,z} \end{Bmatrix}^T \begin{bmatrix} Z^T S Q S Z & Z^T S^T Q B & Z^T S^T Q S N \\ B^T Q S Z & B^T Q B & B^T Q S N \\ N^T S^T Q S Z & N^T S^T Q B & N^T S^T Q S N \end{bmatrix} \begin{Bmatrix} Y \\ q \\ q_{,z} \end{Bmatrix} dz dA \quad (13)$$

Integrating the block matrices in Eq. (13) over the cross-sectional area, the matrix H is obtained and the strain energy variation takes the following form

$$\delta U_e = \int_l \begin{Bmatrix} \delta Y \\ \delta q \\ \delta q_{,z} \end{Bmatrix}^T \begin{bmatrix} H_{11} & H_{12} & H_{13} \\ H_{21} & H_{22} & H_{23} \\ H_{31} & H_{32} & H_{33} \end{bmatrix} \begin{Bmatrix} Y \\ q \\ q_{,z} \end{Bmatrix} dz \quad (14)$$

By performing the integration by parts on the variational terms, which are differentiated with respect to axial coordinate (e.g.  $\delta q_{,z}$ ), Eq. (15) can be obtained.

$$\begin{aligned} \delta U_e = \int_l [\delta \Upsilon H_{11} + \delta q H_{21} \Upsilon - \delta q H_{31} \Upsilon_{,z} + \delta \Upsilon H_{12} q \\ + \delta q H_{13} q - \delta q H_{32} q_{,z} + \delta \Upsilon H_{13} q_{,z} + \delta q H_{23} q_{,z} - \delta q H_{33} q_{,zz}] dz \\ + [\delta q H_{31} \Upsilon + \delta q H_{32} q + \delta q H_{33} q_{,z}]_l \end{aligned} \quad (15)$$

The terms inside the last bracket correspond to the boundary terms, which are needed to satisfy the boundary conditions. As is known from the theory of calculus of variations,  $\delta U_e = 0$  must vanish for arbitrary values of the variational terms  $\delta \Upsilon$  and  $\delta q$ . Hence, the following system of differential equations can be obtained.

$$\begin{bmatrix} 0 & -H_{33} \\ 0 & 0 \end{bmatrix} \begin{bmatrix} \Upsilon \\ q \end{bmatrix}'' + \begin{bmatrix} H_{31} & H_{23} - H_{32} \\ 0 & H_{31} \end{bmatrix} \begin{bmatrix} \Upsilon \\ q \end{bmatrix}' + \begin{bmatrix} H_{21} & H_{21} \\ H_{11} & H_{12} \end{bmatrix} \begin{bmatrix} \Upsilon \\ q \end{bmatrix} = \begin{bmatrix} 0 \\ 0 \end{bmatrix} \quad (16)$$

However, Eq. (16) requires six constraints that should be imposed on the warping displacements and their derivatives (Kashefi et al. 2016) in order to prevent the warping displacement inducing section translations and rotations. The constraints can be introduced by Lagrange multipliers  $\bar{\lambda}$  and the resulting equation can be written as

$$\begin{bmatrix} 0 & -H_{33} & 0 \\ 0 & 0 & 0 \\ 0 & 0 & 0 \end{bmatrix} \begin{bmatrix} \Upsilon \\ q \\ \bar{\lambda} \end{bmatrix}'' + \begin{bmatrix} H_{31} & H_{23} - H_{32} & D \\ 0 & H_{31} & 0 \\ D^T & 0 & 0 \end{bmatrix} \begin{bmatrix} \Upsilon \\ q \\ \bar{\lambda} \end{bmatrix}' + \begin{bmatrix} H_{21} & H_{21} & D \\ H_{11} & H_{12} & 0 \\ D^T & 0 & 0 \end{bmatrix} \begin{bmatrix} \Upsilon \\ q \\ \bar{\lambda} \end{bmatrix} = \begin{bmatrix} 0 \\ 0 \\ 0 \end{bmatrix} \quad (17)$$

The constraint matrix  $D$  introduced in Eq. (17) expresses that the warping and distortional displacements should not contribute to the section translations and rotations and given as

$$D = \begin{bmatrix} I & \cdots & I & \cdots & I \\ h_1 & \cdots & h_i & \cdots & h_n \end{bmatrix} \text{ and } \begin{bmatrix} 0 & 0 & y_i \\ 0 & 0 & -x_i \\ -y_i & x_i & 0 \end{bmatrix} \quad (18)$$

Where  $I$  is the identity matrix,  $h_i$  consists of the coordinates of  $i_{th}$  is the node and  $n$  is the number of nodes in the discretized cross-section. Additionally, Eq. (17) can be written in a compact form by introducing the matrices  $\Psi_2, \Psi_1, \Psi_0$  and the vector  $\Delta$  as follows

$$\Psi_2 \Delta'' + \Psi_1 \Delta' + \Psi_0 \Delta = 0 \quad (19)$$

An exponential solution in the form of  $\Delta = \Delta_e e^{\lambda z} c_e$  can be

assumed and the corresponding eigenvalues  $\lambda$  and eigenvectors  $\Delta_e$  can be obtained (Hansen and Jönsson 2019a). However, the solution to Eq. (19) can be cumbersome if the cross-section is discretized using a dense mesh, which results in a relatively high number of *dofs*. Hence, Eq. (19) can be linearized as given in Eq. (20). The linearized form of the quadratic eigenvalue problem can be solved for the necessary number of eigenmodes (e.g. for the lower energy modes). The solution can be achieved by using MATLAB *eigs* function, which has parallel processing capabilities.

$$\begin{bmatrix} I_s & 0 \\ 0 & \Psi_2 \end{bmatrix} \begin{bmatrix} \Delta \\ \bar{\Delta} \end{bmatrix}' + \begin{bmatrix} 0 & I_s \\ -\Psi_0 & -\Psi_1 \end{bmatrix} \begin{bmatrix} \Delta \\ \bar{\Delta} \end{bmatrix} = \begin{bmatrix} 0 \\ 0 \end{bmatrix} \quad (20)$$

In Eq. (20),  $I_s$  is the identity matrix with appropriate size and  $\bar{\Delta}(z) = \Delta(z)'$ . From the solution of Eq. (19) or (20), the eigenvalues and the corresponding eigenvectors are obtained as the pairs of real eigenvalues and the complex quadruples.

#### 4. Beam Element Stiffness Matrix

Having obtained the cross-sectional displacement modes, standard displacement-based FE beam elements can be formulated using linear or higher-order interpolation functions with  $C^0$  continuity. It should also be mentioned that the interpolation functions with  $C^1$  continuity can also be adopted, yet, the resulting beam element would have higher *dofs*. The inclusion of complex quadruples in the formulation of the beam element stiffness matrix requires dealing with complex numbers. In order to avoid dealing with complex section displacement functions extracted from complex quadruples, real and imaginary parts of an eigenvector corresponding to an eigenvalue with positive real and imaginary parts are adopted separately.

The distortional part of the cross-section displacements  $u^d$  at any material point can now be expressed by the displacement mode constant  $c$  as

$$\begin{bmatrix} u_x^d \\ u_y^d \\ u_z^d \end{bmatrix} = \begin{bmatrix} \varphi_x^1 & \varphi_x^2 & \cdots & \varphi_x^{nm} \\ \varphi_y^1 & \varphi_y^2 & \cdots & \varphi_y^{nm} \\ \varphi_z^1 & \varphi_z^2 & \cdots & \varphi_z^{nm} \end{bmatrix} \begin{bmatrix} c_1 \\ c_2 \\ \vdots \\ c_{nm} \end{bmatrix} \text{ or } u^d = \varphi c \quad (21)$$

where the mode matrix  $\varphi$  contains the eigenvectors, which consists of the corresponding elements of the eigenvector  $\Delta_e$  obtained from the solution of Eq. (19) or (20). The number of modes included in the analysis is indicated by  $nm$ . The section displacement vector  $U$  and the displacement mode constant vector  $c$  within the element domain can be expressed using interpolation functions  $N$ , for section dis-

placements and  $N_d$  for displacement modes constants as

$$\begin{bmatrix} U \\ c \end{bmatrix} = \begin{bmatrix} N_r & 0 \\ 0 & N_d \end{bmatrix} \begin{bmatrix} \hat{U} \\ \hat{c} \end{bmatrix} \text{ or } v = \check{N}\check{v} \quad (22)$$

where  $\hat{U}$  and  $\hat{c}$  are the nodal degrees of freedom. It should be noted that the section displacement vector includes six components while the length of  $c$  depends on the number of displacement modes included in the analysis. Besides, the displacement mode constant vector includes constants for both the real and the imaginary part of the displacement modes. The number of degrees of freedom at a node of the finite element depends on the number of modes included in the analysis. By substituting Eqs. (3), (6) and (23) into Eq. (5) and using the first variation of elastic strain energy, the beam element stiffness matrix can be obtained as

$$K^e = \int_{\mathcal{V}} \sum \int_{A^e} [SZR + B\phi\check{N} + SN\phi\check{N}_{,z}]^T Q[SZR + B\phi\check{N} + SN\phi\check{N}_{,z}] dA^e dz \quad (23)$$

where  $R$  can be expressed as

$$R = \mathcal{L}\check{N} + \check{N}_{,z} \quad (24)$$

## 5. Numerical Results

In this section, several examples, including the beams with open and closed sections made of homogeneous isotropic and anisotropic material, are presented to assess the performance of the proposed method. The results obtained from the proposed method are benchmarked against those from previous studies and/or 3D solid and shell element formulations. The developed 3D beam analysis approach consists of two main parts: a 2D cross-sectional analysis using quadrilateral elements, and a 1D beam finite element (FE) analysis employing either linear or cubic interpolation functions, which can be utilized to analyze beams with any arbitrary cross-section shapes. Cross-sectional displacement modes, including warping and distortion, were calculated by solving a quadratic eigenvalue problem and subsequently integrated into the FE formulation. The proposed FE model was implemented using custom-developed MATLAB code.

### 5.1. End Loaded Cantilever Beam with Channel Section

The first example is a cantilever beam (Figure 2a), which was also analyzed by Hansen and Jönsson (2019b). The cross-sectional shape of the beam is a channel, with a height of 100 mm, a width of 40 mm, and web and flange thicknesses of 3 mm. The elasticity modulus of the beam material is 210 GPa, and Poisson's ratio is 0.3. A load of 50 kN/m shear force is distributed along the web of the tip section.

However, in the present approach, the load is applied at the geometric center as a concentrated shear force and torsional moment. The beam is discretized using 10 three-node FE elements with Lagrange basis shape functions, and the cross-section is meshed using four-node 96 quadrilateral elements as shown in Figure 2c.

The eigenvalues, and the modal values of section strains  $\Upsilon$  calculated from the solution of the eigenvalue problem are given in Figure 3 for the first five cross-section displacement modes. The first and second modes are the warping modes due to coupled torsion and shear effect, the third mode is the 1st shear/bending mode in the  $x$  direction, the fourth mode is the 2nd shear/torsion coupled mode while the fifth mode is the 2nd shear/bending mode (in Table 1).

The calculated displacement modes are also in accordance with the ones presented in Hansen and Jönsson (2019b), except that the first and the second modes presented in this study are similar in shape, yet, the magnitudes of the distortions and the warping displacements are different. As reported by Hansen and Jönsson (2019b), those modes are also the same as unrestrained torsional mode, which is the case for open sections.

The displacement values calculated at point B using only one displacement mode and the first ten displacement modes are presented in Table 2. It should be noted that the first ten displacement modes include ten real parts and nine corresponding imaginary parts of the displacement modes. Hence, a total of nineteen modes are used, yet, the total number of modes will not given hereinafter in order to prevent confusion. Obviously, the calculated displacements reasonably agree with the displacements presented in Hansen and Jönsson (2019b). The differences arise due to the method of applying the external load, and the sign differences result from variations in the direction of coordinate selection. In Hansen and Jönsson (2019b), the load is applied as nodal forces distributed along the web, whereas in this study, the loads are applied at the geometric center as concentrated shear and torsion. Furthermore, the displacement results obtained using only one displacement mode are still in good agreement with results from the analysis in which the first ten displacement modes were used.

The normal and shear stress variations along the cross-section calculated by the proposed beam element for different numbers of displacement modes are given in Figure 4. It is observed that the variations of normal stresses along the web and flange are reasonably in agreement with Abaqus re-

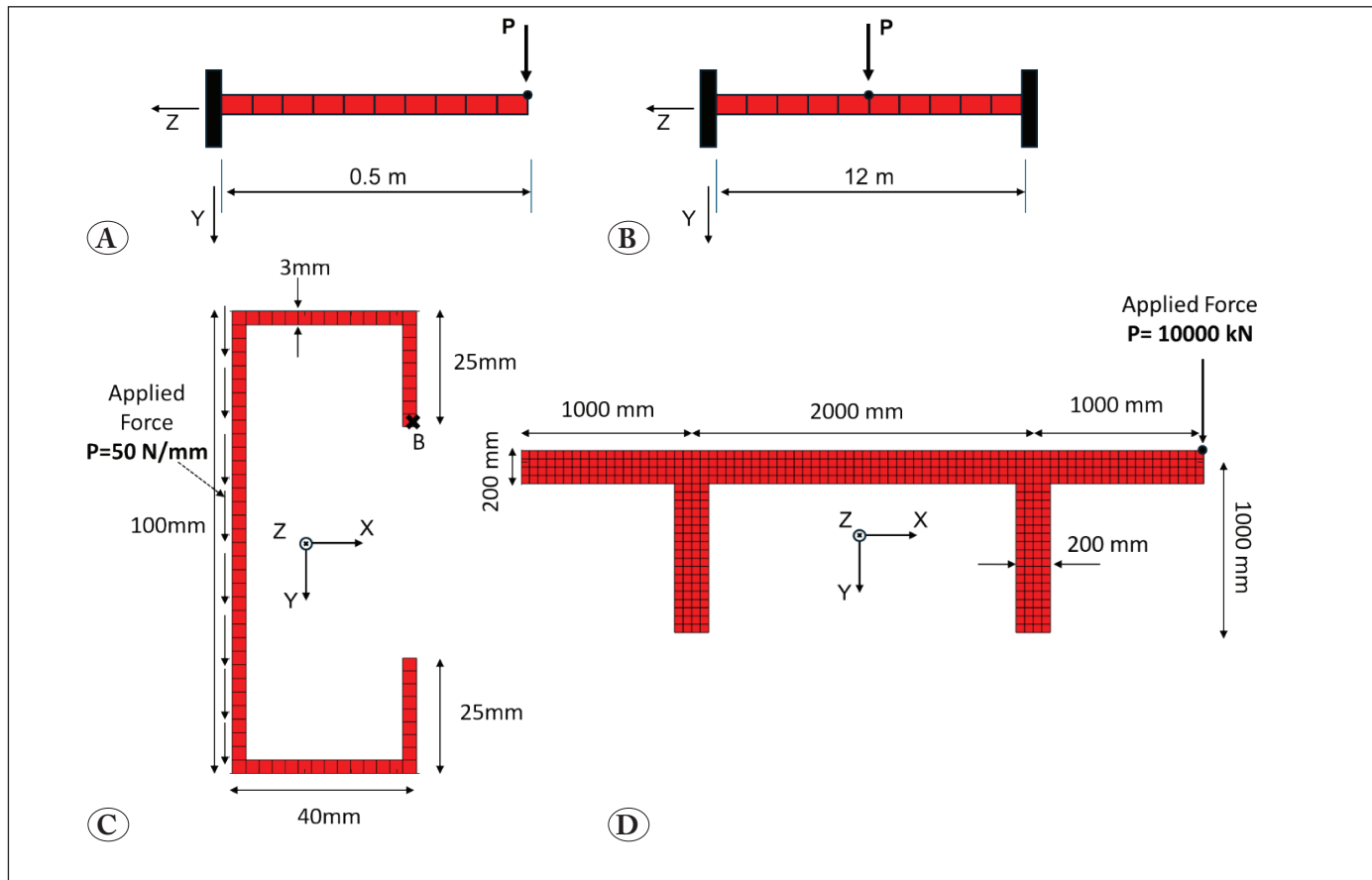


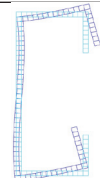

**Figure 2.** The support and loading conditions for **A)** channel and **B)** double T cross-section beams, the geometry and the FE mesh for **C)** channel section, **D)** double T section.

**Table 1.** Mode details and mode shapes.

Real Mode	Hansen and Jönsson, 2019b	Present	Present - Mode Shape
1	Warping	Warping mode (coupled torsion and shear)	
2	Warping	Warping mode (coupled torsion and shear)	
3	Shear/bending	1st shear/bending (in x-direction)	



**Table 1.** Cont.

4	Shear/torsion	2nd shear/torsion	
5	Shear/bending	Shear/bending	

**Table 2.** Displacement at the upper right corner of box section ( $x=21.5\text{mm}$ ,  $y=51.5\text{mm}$ ) (units are in mm)

Displacement	Hansen and Jönsson (2019b)	Hansen and Jönsson (2019b)- Abaqus	Present-number of modes=10	Present-number of modes=1
$u_x$	1.1055	1.1107	0.7740	0.8331
$u_y$	-2.9155	-2.9324	3.2251	3.1389
$u_z$	-0.1488	-0.1501	0.1415	0.1399

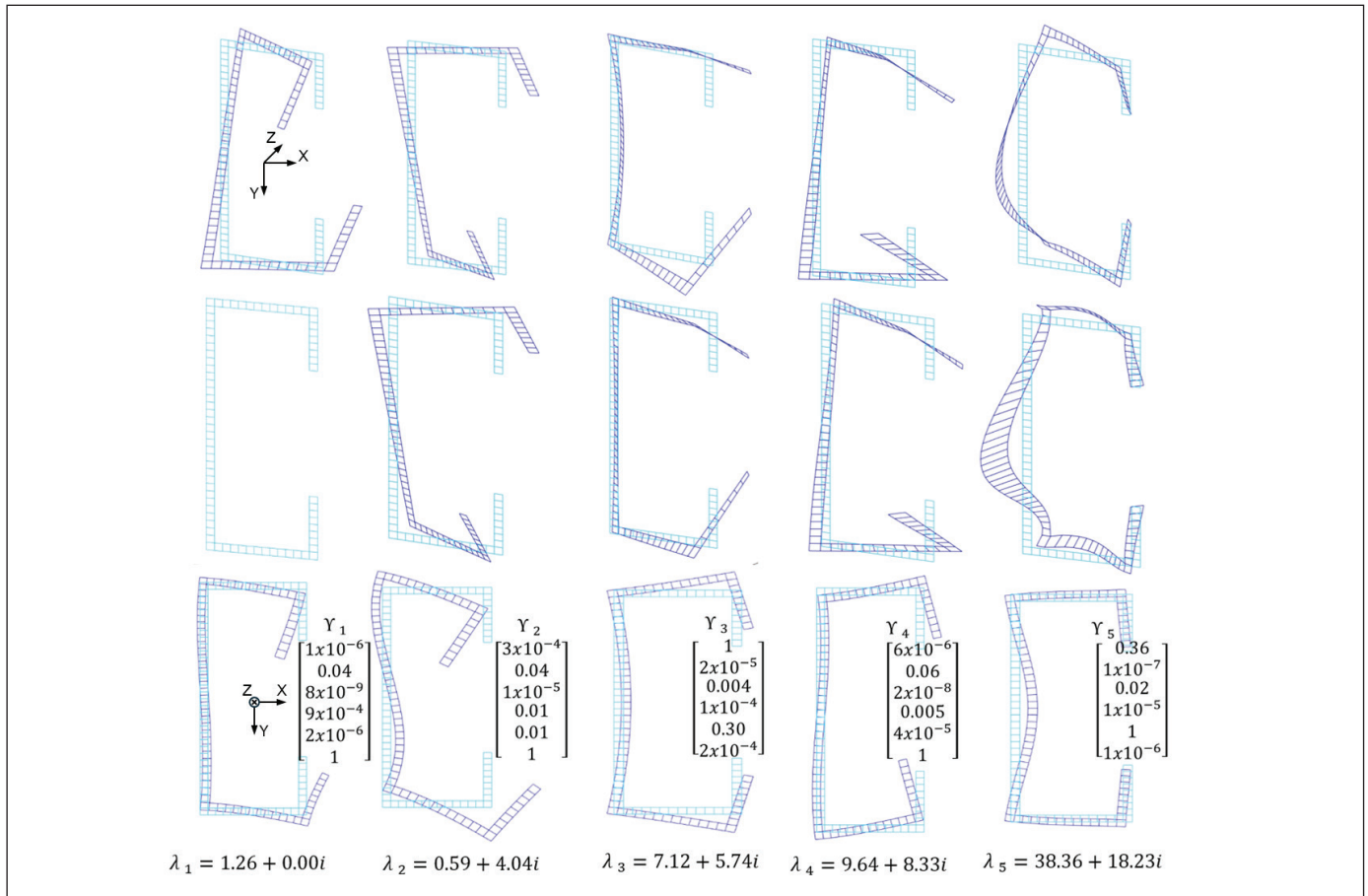


**Figure 3.** First five cross-section displacement modes of the channel section. The first and second rows illustrate the real and imaginary parts of the warping (out-of-plane) displacements, while the third row illustrates the transverse (in-plane) displacement.

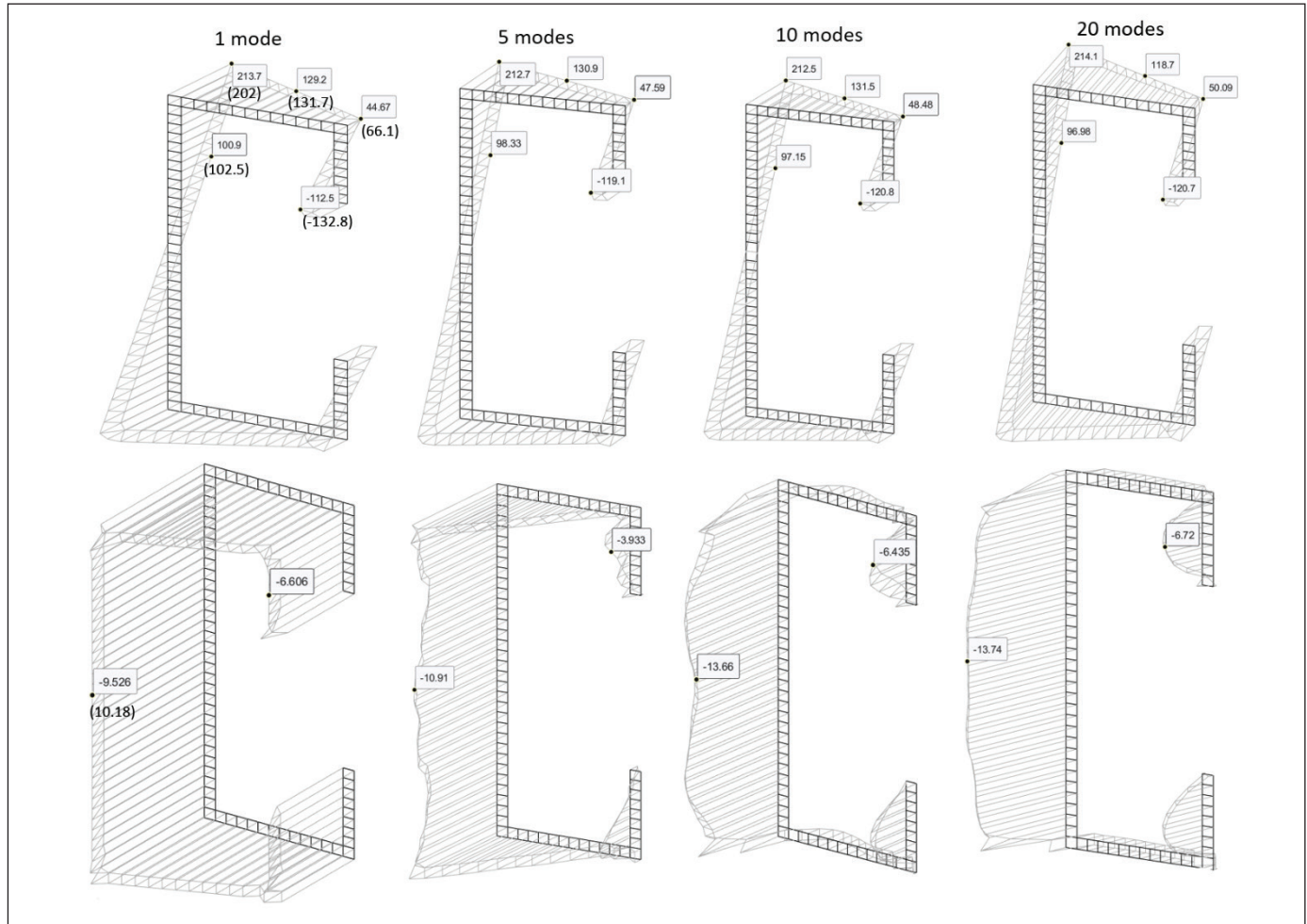


**Figure 4.** Stress distribution on channel cross-section at 10 mm from the support. Normal stress and shear stress distributions are given in first and second rows, respectively. The Abaqus results presented in Hansen and Jönsson (2019b) are given in parentheses.

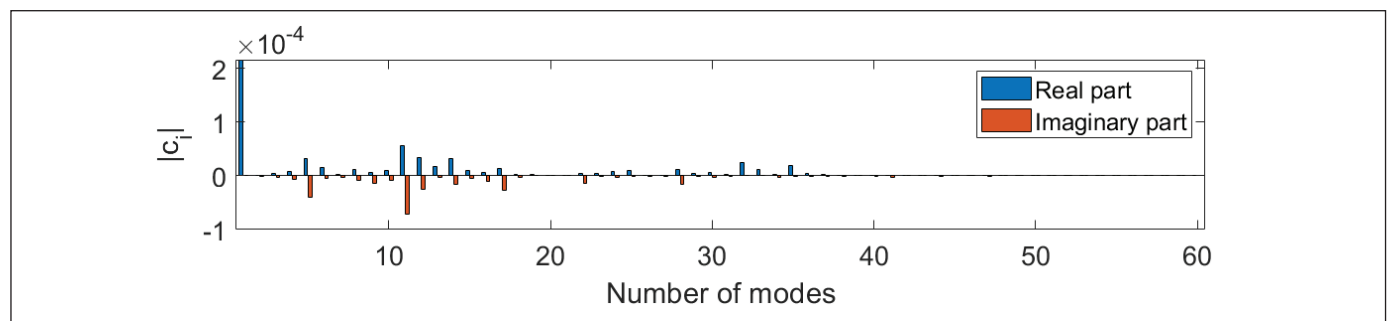


**Figure 5.** Displacement mode constants for channel section.

sults. Moreover, the normal stress variations do not significantly differ when higher displacement modes are included. The inclusion of the first mode gives sufficiently good predictions for normal stress variation. However, this is not the case for the shear stress variations. Regarding the predicted shear stress distributions, considerable discrepancies are observed between the results from the analysis where differ-

ent numbers of modes are included. Hence, it is noted that higher-order modes should be included in the calculation of shear stress variations for more accurate predictions.

The contributions from each mode (the displacement mode constants) are illustrated in Figure 5. However, it is worth noting that the values of the constants presented in Figure

5 may change depending on the normalization procedure adopted for the displacement modes. In this study, the displacement modes were simply normalized with respect to their maximum values. Obviously, the first mode has a significant contribution to the deflected shape, which is also consistent with the displacements presented in Table 2. This is also true for the normal stress distribution given in Figure 4. Besides, there are some higher modes of which their constants take notable values. However, these modes largely affect the shear stress variations rather than the deflected shape and normal stress variations as demonstrated previously.

## 5.2. Double T Cross Section

The second example concerns a beam with a double T cross-section studied by Ferradi and Cespedes (2014). Both ends of the beam are fixed, whereas a 10000 kN eccentric load is applied at the corner of the mid-span section (Figure

1b), which causes bending/shear with non-uniform torsion. Young's modulus and Poisson ratio are assumed to be  $E=40$  GPa and  $\nu=0$ , respectively. The beam was analyzed by using ten three-node finite elements in the axial directions, and 464 quadrilateral elements were used in cross-section discretization (Figure 1d).

Computing the corresponding eigenvalue problem and selecting the appropriate modes, the total number of 1761 displacement modes was obtained. The first five displacement modes are presented in Figure 6. Observing the displacement mode shapes and the modal section strain values, it can be deduced that the first mode is a coupled shear/torsion warping mode. This is expected since the section is monosymmetric, which means shear and geometric centers are not coincident. The second mode is the shear/bending mode in the y direction. The third mode is the second shear/torsion warping mode. The fourth mode is the coupled ex-

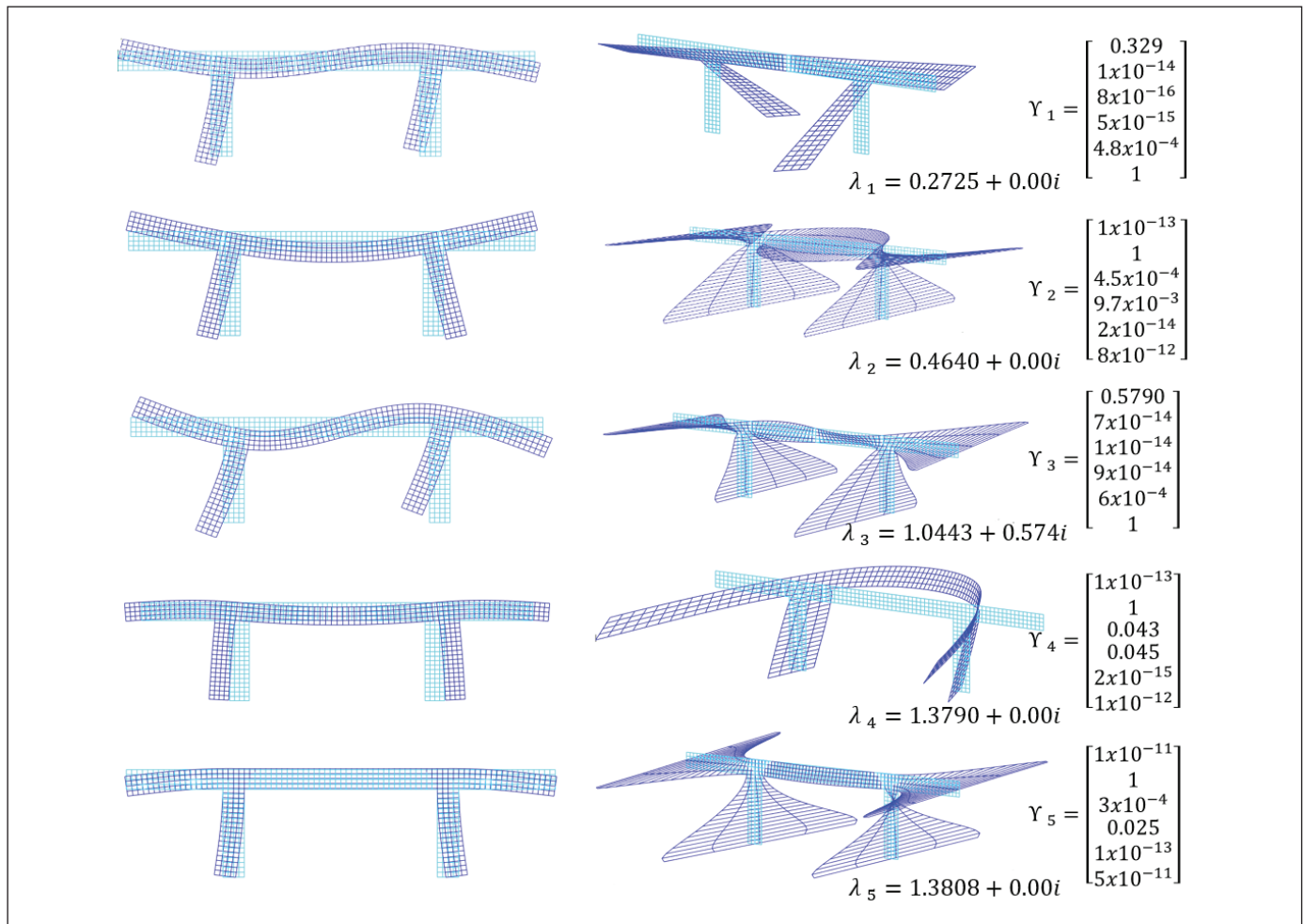


**Figure 6.** First five displacement modes of double T section. The first and second columns are the in-plane and warping displacement modes, respectively. The modes are ordered from top to bottom in increasing order.

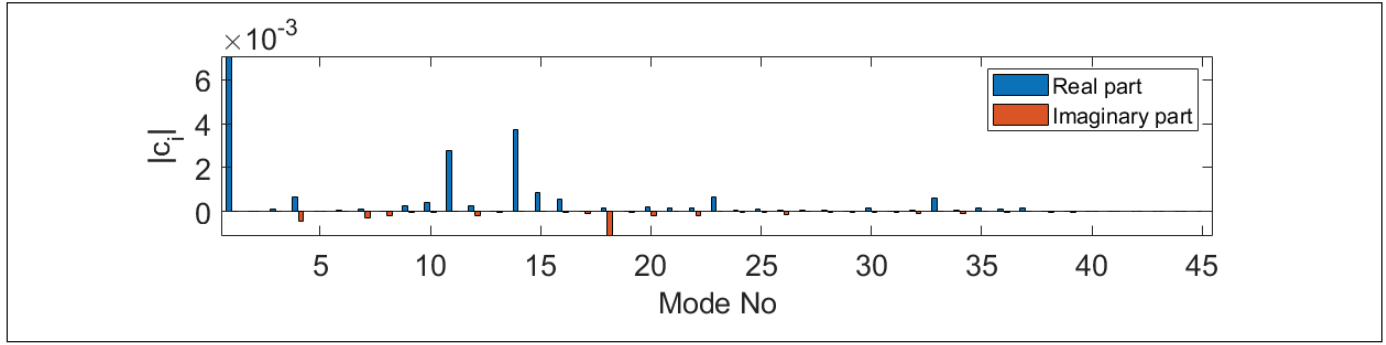


**Figure 7.** The absolute value of displacement mode constants for the deck section.

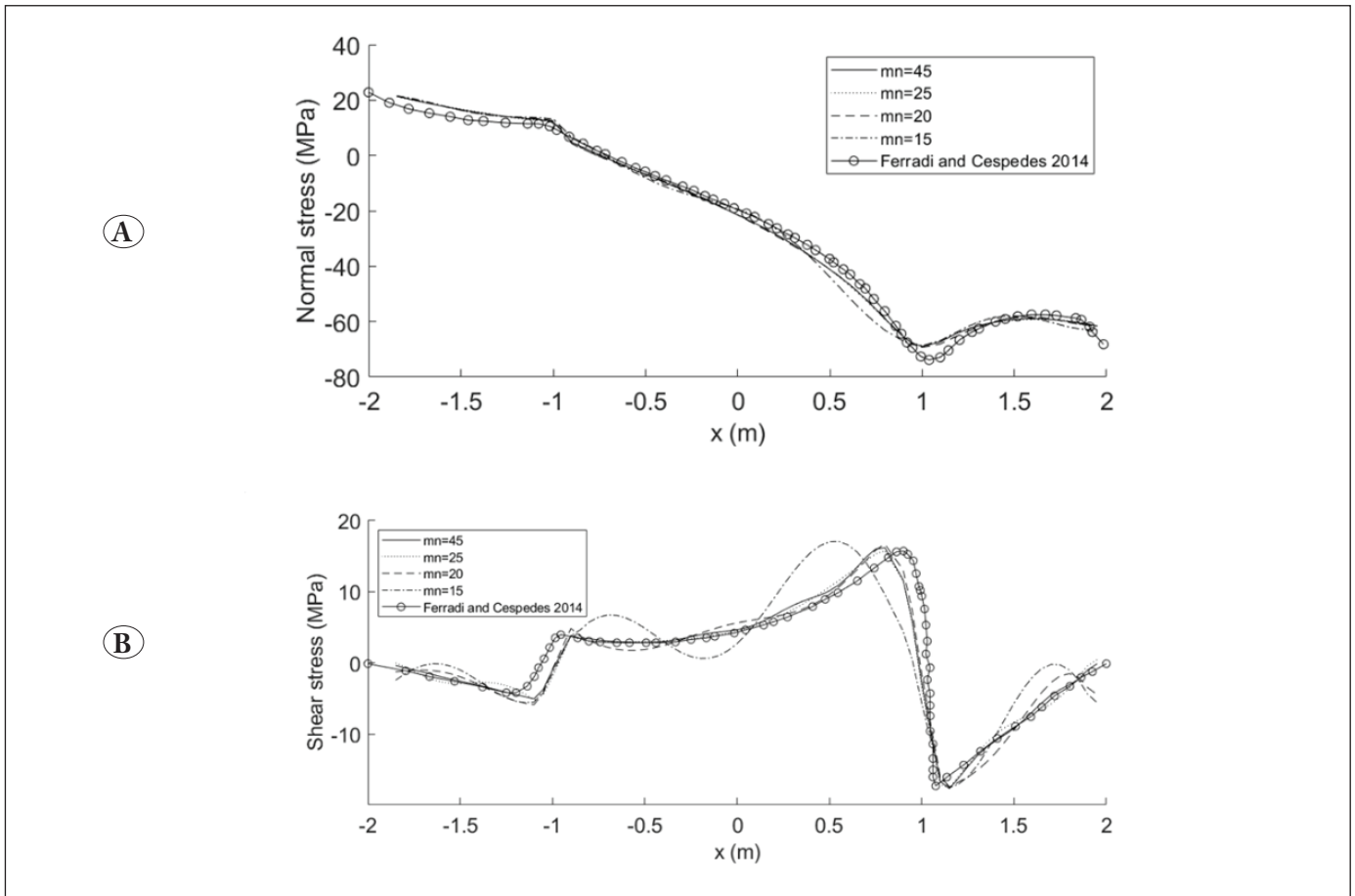


**Figure 8.** Stress variations along the flange of double T section **A)** normal stresses **B)** shear stresses.

tension and shear/bending mode, and the fifth mode is the second shear/bending mode in the y direction. The mode constants presented in Figure 7 show that the first warping mode contributes significantly. In addition, the contribution of some higher modes (modes between mode 10 and mode 20) is also obvious, while the contributions from imaginary parts are less significant in this example.

The normal and shear stress variations along the flange of the double T cross-section given in Figure 8 demonstrate the accuracy of the stress field predictions. The stress variations obtained from the present beam element and the results of Ferradi and Céspedes (2014) agree well. However, the accuracy starts to decrease when only the first fifteen displacement modes are included in the analysis. Specifically, dramatic changes occur in shear stress variations, while

**Table 3.** The displacements calculated at the mid-span of the beam considering the contributions from different numbers of higher-order displacement modes (units in translation and rotation are m and radian, respectively).

Displacement / mode number	45	25	20	15	10	5	1
$u_x$	-0.00982	-0.00981	-0.00977	-0.00934	-0.00934	-0.010	-0.0099
$u_y$	0.0263	0.0262	0.0259	0.0252	0.0245	0.0235	0.0232
$\theta_z$	0.0380	0.0377	0.0376	0.0358	0.0346	0.0325	0.0324

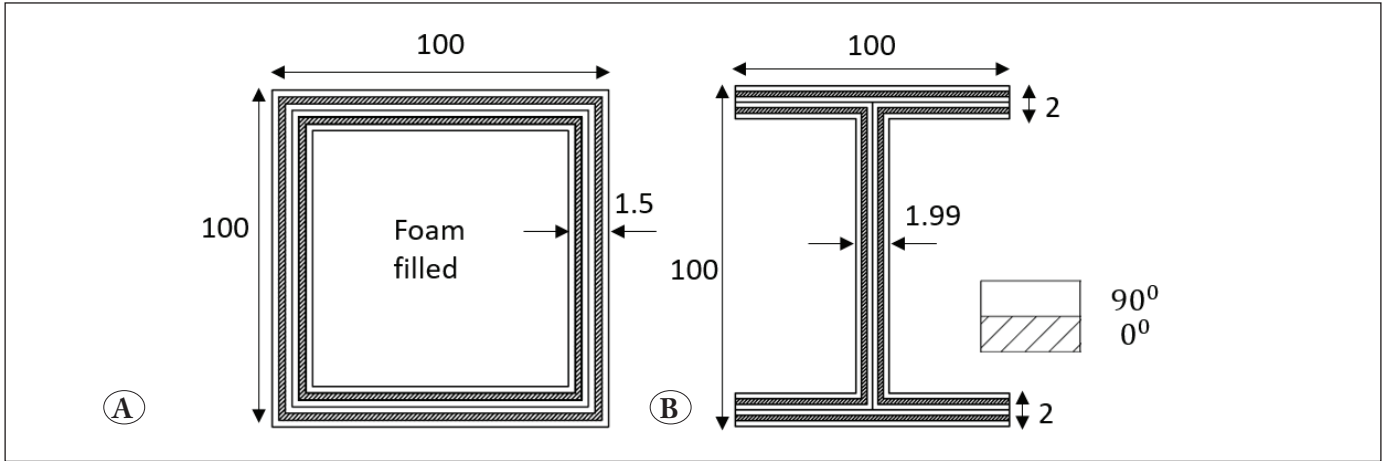


**Figure 9.** Geometry and fiber orientation of laminated composite **A)** box cross-section **B)** I cross-section.

the normal stress variations are still reasonably accurate. Furthermore, the displacement results given in Table 3 indicate that the beam nodal displacements can be predicted with reasonable accuracy even in the case when only one mode is involved in the deformation analysis.

### 5.3. Thin-walled Composite Closed Box Beam

A laminated thin-walled composite cantilever beam is analyzed implementing the presented approach in this study, and the results are compared with the those of Islam et al. (2021). This beam has also been analyzed considering the same section with a polymer foam as an in-filled material. The geometry and the lamina configuration are presented in Figure 9. The beam was analyzed under 1 kN transverse shear load and 1 kNm torsional moment, respectively. The material properties of all layers are:  $E_1 = 48.5 \text{ GPa}$ ,  $E_2 = E_3 = 5.5 \text{ GPa}$ ,  $G_{12} = G_{13} = 2.5 \text{ GPa}$ ,  $G_{23} = 2 \text{ GPa}$ ,  $\nu_{12} = \nu_{13} = \nu_{23} = 0.33$  while the material properties of the foam are:  $E = 0.400 \text{ GPa}$ ,  $G = 0.097 \text{ GPa}$  and  $\nu = 0.4$ .

The numerical analysis results of the composite beam revealed that the contribution of higher modes is more significant than the lower-order displacement modes. The displacement mode constants presented in Figure 10 clearly

indicate the importance of higher-order modes. Particularly, the index numbers of the most pronounced constants for the section with foam filled are higher than 40. Besides, some imaginary parts of the displacement modes of the cross-section without foam filled seem to be more significant than the real part, while the real parts of the displacement modes are more dominant for the cross-section with foam filled. The first four dominant displacement modes are presented in Figure 11. The first warping mode (given in the second row of Figure 11a.), which is the lowest energy mode contributes significantly to the cross-section without foam filled. Otherwise, the most pronounced displacement modes are higher energy modes for the cross section with foam filled.

Having realized that the high energy modes contribute significantly to the deformation field, using the proposed approach numerical analyses have been carried out considering different numbers of highly contributed displacement modes. The displacement results obtained at the free end of the cantilever beam using the proposed calculation approach with different mode numbers are presented in Table 4, compared to those in the literature (Islam et al. 2021). As seen, the results of the present beam element agree well with



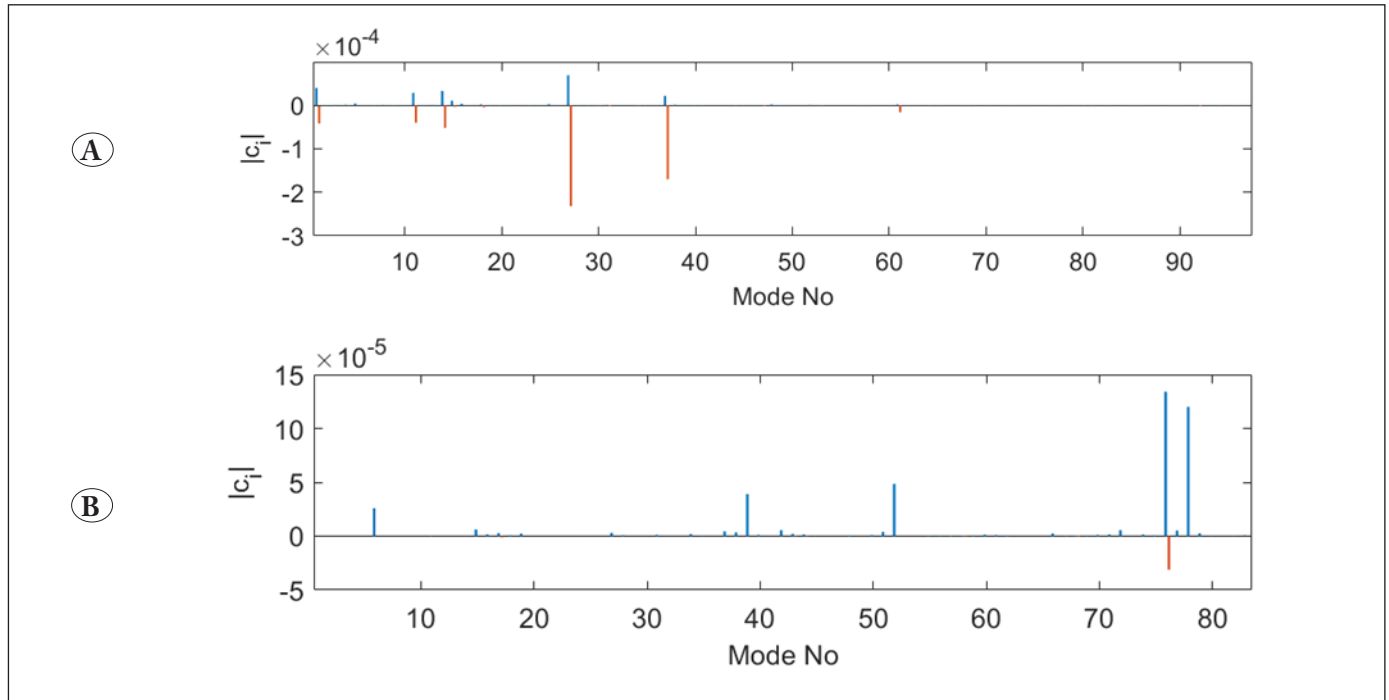


**Figure 10.** Displacement mode constants obtained from the analysis of the beam when 1 kNm torsional moment is applied **A)** section without foam filled **B)** section with foam filled.

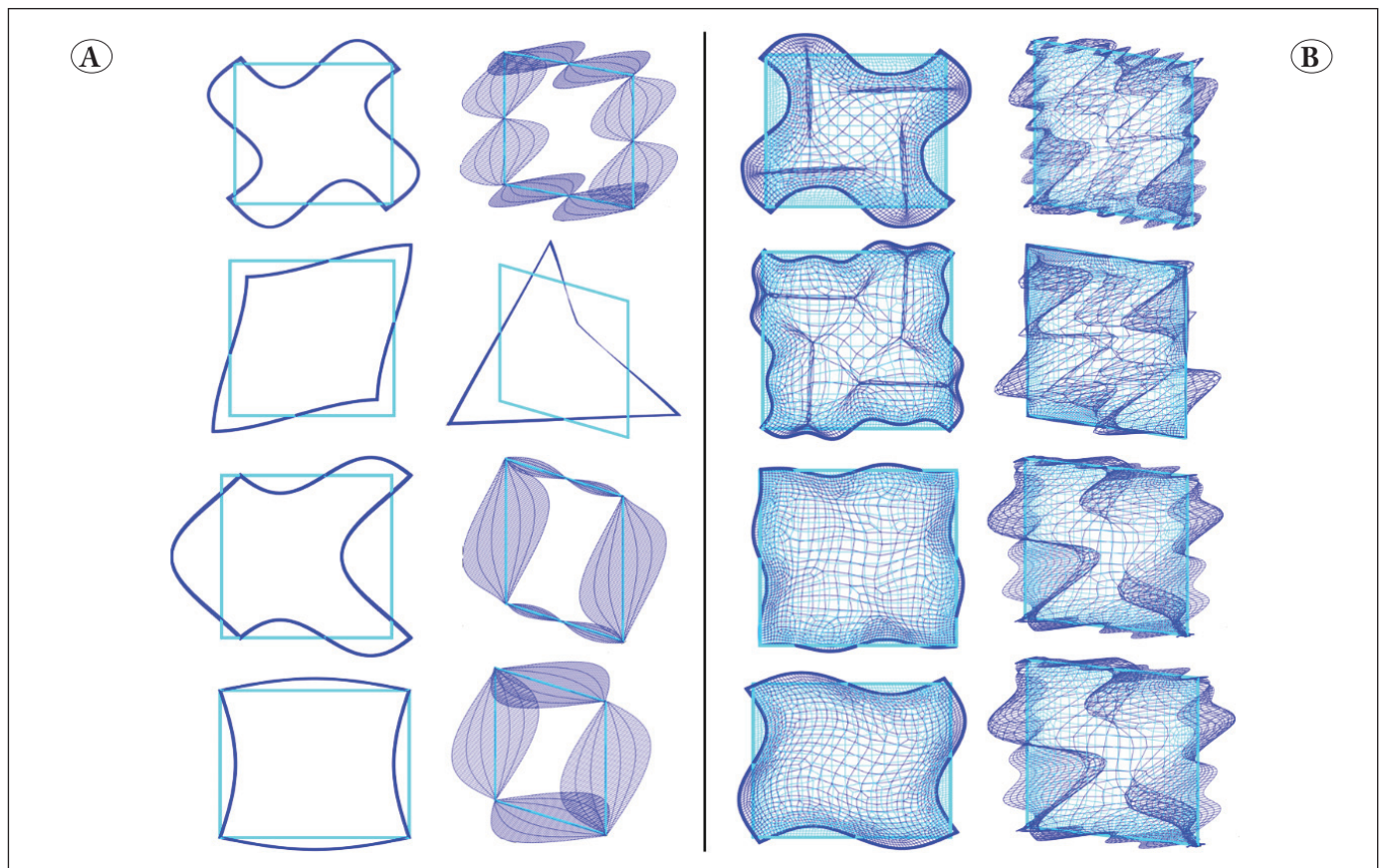


**Figure 11.** The first four most pronounced transversal and warping displacement modes **A)** without foam filled **B)** with foam filled.

**Table 4.** Tip displacements calculated using different numbers of displacement modes (units in translation and rotation are mm and radian, respectively).

Loading (Displacement component)	Condition	Number of modes				
		Islam et al. (2021) (Abaqus)	mn=20	mn=10	mn=5	mn=2
Transverse force ( $u_y$ )	w/o foam	11.609 (11.46)	11.64	11.33	11.28	10.83
	w/ foam	9.74 (9.58)	9.78	9.74	9.72	9.72
Torsional moment ( $\theta_z$ )	w/o foam	27.6 (28.06)	27.8	27.76	26.71	26.24

the results of Islam et al. (2021) when the first 20 displacement modes are used. Besides, the difference between the results is not considerable even when the first two modes are considered in the calculations. In addition, the discrepancies between the results from different number modes are so small for the cross section with foam filled. This is due to the fact that the foam introduces additional stiffness to

the cross-section, which results in a lower deformation state that can be represented by a few displacement modes. As seen in Figure 12, the normal stress distribution calculated at the fixed end of the cross-section without foam shows that the shear lag effect can be captured properly. The calculated maximum normal stress is almost identical to the maximum stress value reported in Islam et al. (2021), which is given as 79.2 MPa.

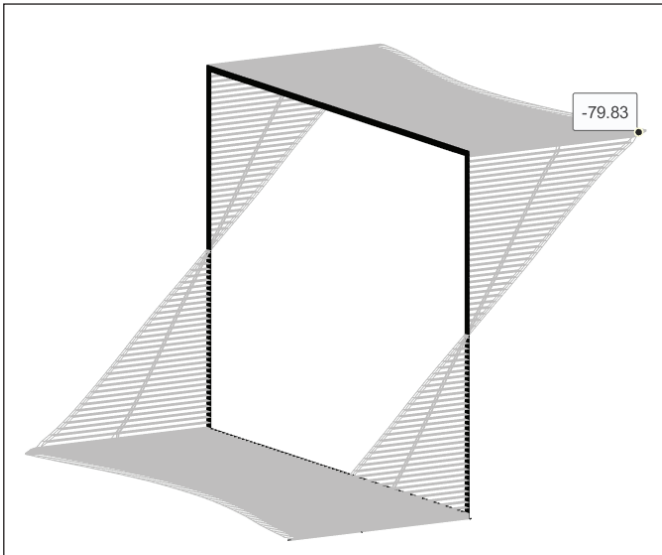


**Figure 12.** Normal stress variation calculated at the fixed end of the composite box beam.

#### 5.4. Thin-walled Composite I Beam

The last example is the laminated composite cantilever I beam loaded at the free end with a concentrated shear load (Figure 9b). In order to verify the results under non-uniform torsion, the analyses were also carried out considering that the warping *dofs* at the fixed end are constrained and a uniformly distributed torsion is applied along the beam. The material characteristics are the same as in the previous example. The cross-section was discretized using 2568 quadrilateral elements, and the beam was divided into 10 three-node finite elements in the longitudinal direction.

The displacement mode constants presented in Figure 13 show that the contributions from higher modes are substantially significant compared to lower-order modes. The first four most pronounced cross-section displacement modes are presented in Figure 14. The transverse displacement in the y direction was calculated using a different number of

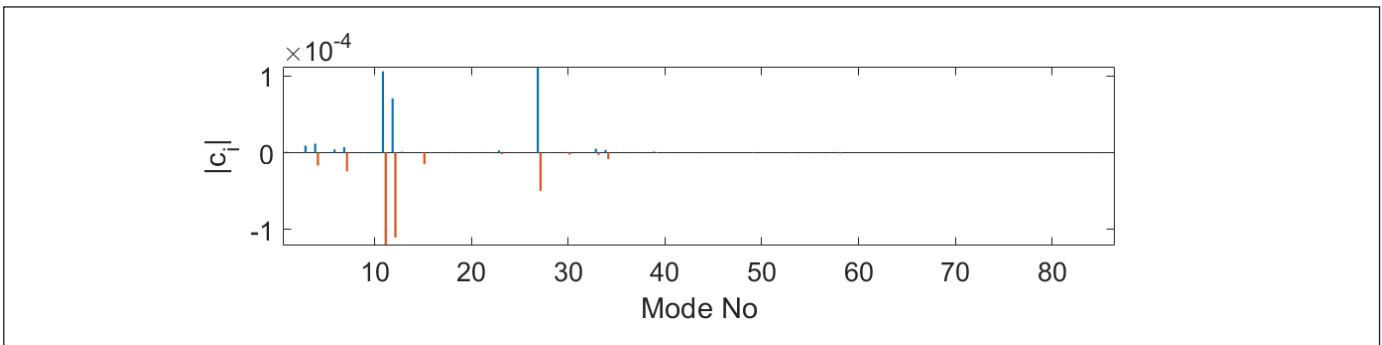


**Figure 13.** Displacement mode constants obtained from the analysis of the I beam under 1 kN concentrated shear load.

displacement modes and compared with the results of Islam et al. (2021) in Figure 15a. Obviously, the results are identical to those of Islam et al. (2021). Nevertheless, the accuracy of the results decreases when the number of displacement modes less than ten is considered in the analysis. The normal stress distribution given in Figure 16 demonstrates that the shear lag effect is correctly predicted. The maximum normal stress was found to be 72.47 MPa, compared to 71.67 MPa in Islam et al. (2021).

In order to verify the results under the effect of non-uniform torsion, 1 Nm/m distributed moment was applied and the warping degrees of freedom at the fixed end were constrained. The variation of twisting angle along the beam is compared with the results of a shell element model creat-

ed in commercial code ANSYS. The shell model includes 115962 *dofs*, whereas the proposed beam element has 506 *dofs*, which results from the inclusion of six section displacements, and ten real and ten imaginary displacement mode constants at each node of the beam element. As seen in Figure 15b, the results of the presented beam element well-agree with the results of ANSYS shell element model. There is a slight discrepancy in the stress prediction around the flange tips, which can be improved by adopting a finer mesh.

## 6. Conclusion

In this study, an efficient higher-order 3D beam element formulation, which capable of accurately predicting the stress and deformation fields, was presented. The formulation can

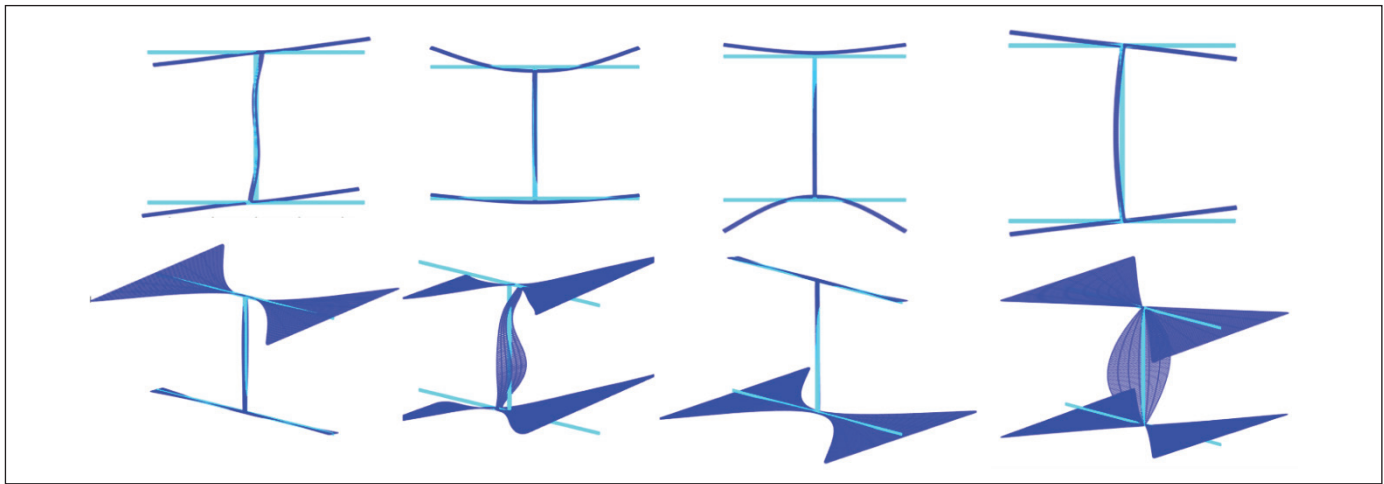


**Figure 14.** The first four most pronounced transversal (first row) and warping (second row) displacement modes for the composite I cross-section.

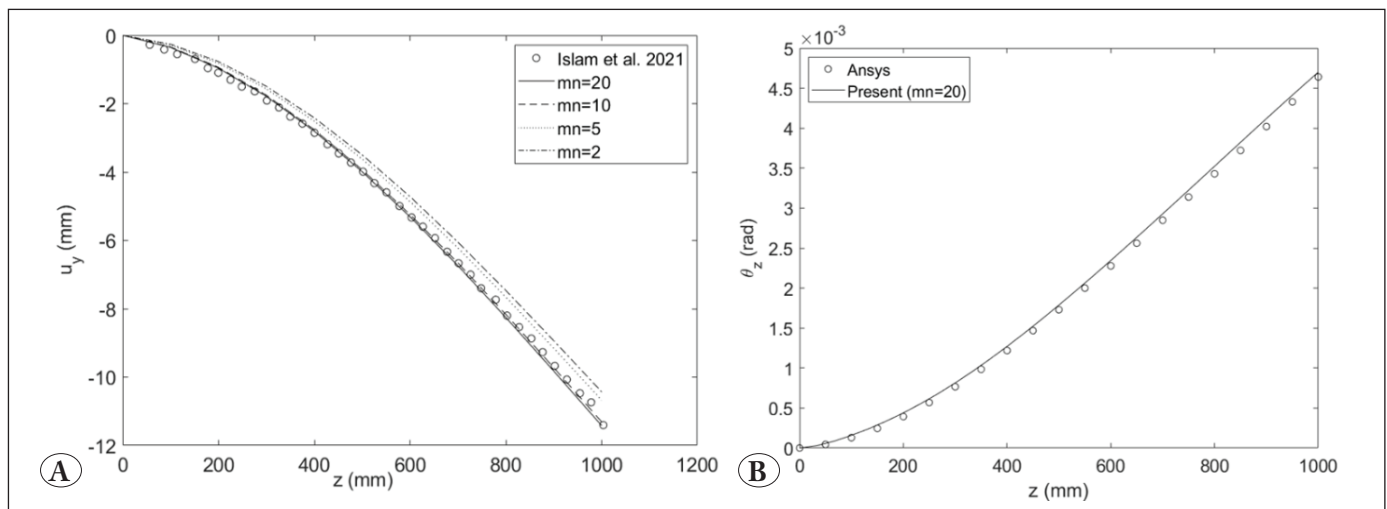


**Figure 15.** Displacement variation along the beam under **A)** transverse shear loading **B)** distributed torsion.

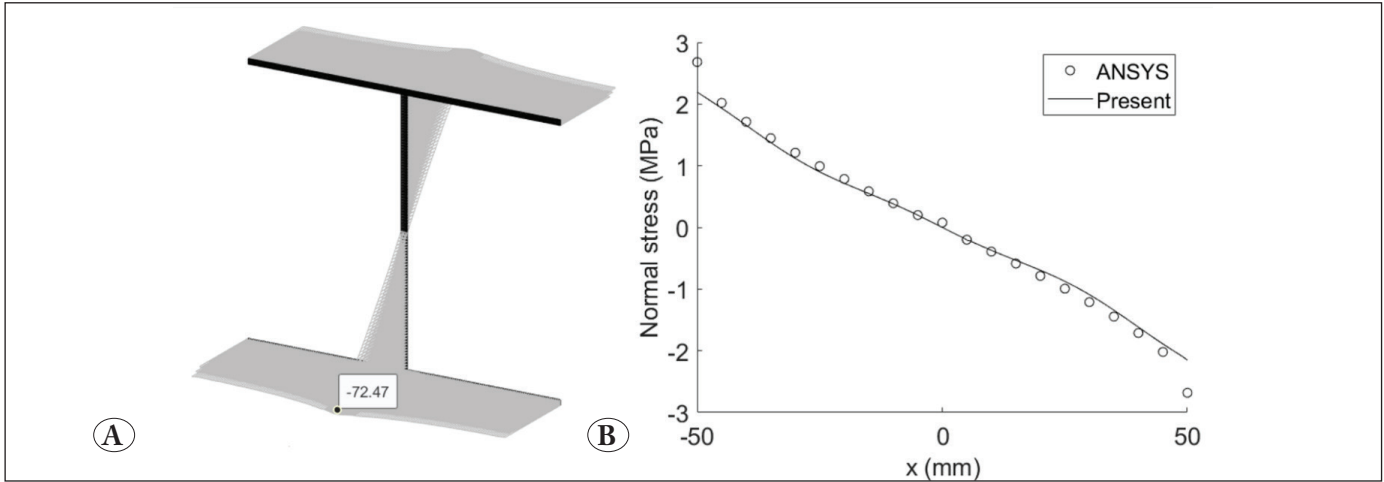


**Figure 16.** Normal stress distribution at the fixed end under **A)** transverse shear loading **B)** distributed torsion (variation along the flange).

be used to analyze the beams with arbitrary cross-section shapes made of isotropic and anisotropic materials. A higher order representation of stress and deformation field was achieved using higher order cross-sectional displacement modes such as distortional and warping modes. The formulation relies on a cross-sectional analysis and related quadratic eigenvalue problem, which generally results in complex eigenvectors. In order to avoid dealing with complex numbers in the calculations, both the real and the imaginary parts of the eigenvectors are assumed to be the components of the deformation field and are included in the analysis using separate constants. The constants of the eigenvectors together with six section displacements are introduced as the degrees of freedom of the beam element. The developed beam element does not have any ad-hoc assumptions and is applicable to any isotropic or laminated composite beams with arbitrary cross-sections.

The performance of the formulation has been validated through several examples from the literature. It was observed that the inclusion of lower-order cross-sectional displacement modes is sufficient to accurately predict the stress and deformation fields of beams made of isotropic material. However, higher-order modes become more dominant in the case of beams made of laminated composite materials. Additionally, few displacement modes are required to accurately predict the global displacements and normal stress variations on the beam's cross-section, while higher order displacement modes are to be included in order to reasonably predict the shear stress variations. Since the described cross-sectional analysis procedure is performed only once before the structural analysis, the proposed beam element is computationally cost-effective and requires substantially

fewer degrees of freedom compared to corresponding shell and solid element models. Hence, it can be used in the analysis of complex 3D structural and mechanical systems, where the cross-sectional distortions and warping are significant and can lead to non-negligible errors when ignored. As a result, all the examples presented in this study clearly indicate that the proposed beam element can predict the stress and deformation field for various cross-section and material properties with reasonable accuracy.

**Author contribution:** **Yıldırım Serhat Erdoğan:** Conceptualization, Methodology, Formal analysis, Visualization, Review and Editing. **Mehmet Ada:** Conceptualization, Methodology, Formal analysis, Visualization, Writing.

**Acknowledgment:** The authors declared no potential conflicts of interest with respect to the research, authorship, and/or publication of this article.

## 7. References

- Ádány, S., Schafer, BW. 2014. Generalized constrained finite strip method for thin-walled members with arbitrary cross-section: Primary modes, *Thin-Walled Structures*, 84: 150-169. doi: 10.1016/j.tws.2014.06.001.
- Addessi, D., Di Re, P., Cimarello, G. 2021. Enriched beam finite element models with torsion and shear warping for the analysis of thin-walled structures. *Thin-Walled Structures*, 159:107259 doi:10.1016/j.tws.2020.107259.
- Barbero, EJ. 2018. *Introduction to Composite Material Design*. CRC Press.
- Barsoum, RS., Gallagher, RH. 1970. Finite element analysis of torsional and torsional flexural stability problems. *International Journal for Numerical Methods in Engineering*, 2:335-352. doi: 10.1002/nme.1620020304.



- Bauld NR., Tzeng, LS. 1984.** A Vlasov theory for fiber-reinforced beams with thin-walled open cross sections. *International Journal of Solids and Structures*, 20(3):277-297. doi:10.1016/0020-7683(84)90039-8.
- Bažant, ZP., El Nimeri, M. 1973.** Large-Deflection Spatial Buckling of Thin-Walled Beams and Frames. *Journal of the Engineering Mechanics Division*, 99(6):1259-1281. doi: 10.1061/JMCEA3.0001837.
- Berdichevskii, VL. 1979.** Variational-asymptotic method of constructing a theory of shells. *Journal of Applied Mathematics and Mechanics*, 43(4): 711-736. doi:10.1016/0021-8928(79)90157-6.
- Bianco, MJ., Könke, C., Habtemariam, A., Zabel, V. 2018.** Exact finite element formulation in generalized beam theory. *International Journal of Advanced Structural Engineering*, 10:295-323. doi:10.1007/s40091-018-0199-8.
- Borri, M., Merlini, T. 1986.** A large displacement formulation for anisotropic beam analysis. *Meccanica*, 21:30-37. doi:10.1007/BF01556314.
- Carrera, E., Giunta, G., Petrolo, M. 2011.** *Beam Structures: Classical and Advanced Theories*. John Wiley & Sons, 2011.
- Cesnik, .ES., Hodges, DH. 1997.** VABS: A new concept for composite rotor blade cross-sectional modeling. *Journal of the American Helicopter Society*, 42(1): 27-38. doi:10.4050/JAHS.42.27.
- Davies, JM., Leach, P. 1994.** First-order generalised beam theory. *Journal of Constructional Steel Research*, 31(2-3):187-220. doi:10.1016/0143-974X(94)90010-8.
- Deo, A., Yu, W. 2020.** Thin-walled composite beam cross-sectional analysis using the mechanics of structure genome. *Thin-Walled Structures*, 152:106663. doi:10.1016/j.tws.2020.106663.
- Dhadwal, MK., Jung, SN. 2019.** Multifield variational sectional analysis for accurate stress computation of multilayered composite beams. *AIAA J.*, 54(4): 1702-1714. doi:10.2514/1.J057384.
- Dikaros, IC., Sapountzakis, EJ. 2014.** Generalized warping analysis of composite beams of an arbitrary cross section by BEM. I: theoretical considerations and numerical implementation *Journal of Engineering Mechanics*, 140(9): (2014):04014062. doi:10.1061/(ASCE)EM.1943-7889.0000775.
- Erkmen, RE., Mohareb, M. 2006.** Torsion analysis of thin-walled beams including shear deformation effects. *Thin-Walled Structures*, 44(10):1096-1108. doi:10.1016/j.tws.2006.10.012.
- Evseev, EG., Morozov, EV. 1997.** Explicit finite difference method in the dynamic analysis of composite structures. *Composite Structures* 39(3-4): 215-221. doi:10.1016/S0263-8223(97)00115-3.
- Ferradi, MK., Cespedes, X. 2014.** A new beam element with transversal and warping eigenmodes. *Computers and Structures*, 131:12-33 doi:10.1016/j.compstruc.2013.10.001.
- Gabbianelli, G. 2021.** Applied element modelling of warping effects in thin-walled C-shaped steel sections. *Buildings*, 11(8):328. doi:10.3390/buildings11080328.
- Giavotto, V., Borri, M., Mantegazza, P., Ghiringhelli, G., Car-maschi, V., Maffioli, GC., Mussi, F. 1983.** Anisotropic beam theory and applications. *Computers and Structures*, 16(1-4):403-413. doi:10.1016/0045-7949(83)90179-7.
- Hansen, AB., Jönsson, J. 2019a.** A thin-walled beam element based on semi-analytical solution modes. *Thin-Walled Structures*, 144:106344. doi:10.1016/j.tws.2019.106344.
- Hansen, AB., Jönsson, J. 2019b.** Displacement modes of a thin-walled beam model with deformable cross sections. *Thin-Walled Structures*, 141:576-592. doi:10.1016/j.tws.2019.01.052.
- Hodges, DH. 2006.** *Nonlinear Composite Beam Theory*. American Institute of Aeronautics and Astronautics, Reston, VA.
- Islam, A., Sheikh, AH., Bennett, T., Thomsen, OT. 2021.** An efficient model for laminated composite thin-walled beams of open or closed cross-section and with or without in-filled materials. *Composites Structures*, 256:112998. doi:10.1016/j.compstruct.2020.112998.
- Jang, GW., Kim, MJ., Kim, YY. 2012.** Analysis of thin-walled straight beams with generally shaped closed sections using numerically determined sectional deformation functions. *Journal of Structural Engineering*, 138(12):1427-1435. doi:10.1061/(ASCE)ST.1943-541X.0000582.
- Jönsson, J. 1999.** Distortional theory of thin-walled beams. *Thin-Walled Structures*, 33(4): 269-303. doi:10.1016/S0263-8231(98)00050-0.
- Jönsson, J., Andreassen, MJ. 2011.** Distortional eigenmodes and homogeneous solutions for semi-discretized thin-walled beams. *Thin-Walled Structures*, 49:691-707. doi:10.1016/j.tws.2010.12.009.
- Kashefi, K., Sheikh, A., Ali MM., Griffith, M. 2016.** An efficient modelling approach based on a rigorous cross-sectional analysis for analysing box girder bridge superstructures. *Advances in Structural Engineering*, 19(3):513-528. doi:10.1177/1369433216630121.
- Kassab, MP., Campello, EMB., Pimenta, PM. 2023.** Advances on kinematically exact rod models for thin-walled open-section members: Consistent warping function and nonlinear constitutive equation. *Computer Methods in Applied Mechanics and Engineering*, 407:115933. doi:10.1016/j.cma.2023.115933.



- Krajcinovic, D. 1969.** A Consistent Discrete Elements Technique for Thinwalled Assemblages, *International Journal of Solids and Structures* 5(7):639-662, doi: 10.1016/0020-7683(69)90085-7.
- Lee, J., Lee, S. 2004.** Flexural-torsional behavior of thin-walled composite beams. *Thin-Walled Structures*, 42(9): 1293-1305. doi:10.1016/j.tws.2004.03.015.
- Lee, J. 2005.** Flexural analysis of thin-walled composite beams using shear-deformable beam theory. *Composite Structures*, 70(2): 212-222. doi:10.1016/j.compstruct.2004.08.023.
- Lezgy-Nazargah, M., Vidal, P., Polit, O. 2021.** A quasi-3D finite element model for the analysis of thin-walled beams under axial-flexural-torsional loads. *Thin-Walled Structures*, 164:107811. doi:10.1016/j.tws.2021.107811.
- Liang, K., Mu, J., Li, Z. 2024.** A novel reduced-order method using mixed nonlinear kinematics for geometrically nonlinear analysis of thin-walled structures. *Computer Methods in Applied Mechanics and Engineering*, 421:116756. doi:10.1016/j.cma.2024.116756.
- Liu, H., Wang, W., Deng, L., He, Y. 2023.** Inelastic buckling analysis of cold-formed steel members with residual stresses based on CFSM. *Structures*, 56:104871. doi: 10.1016/j.istruc.2023.06.142.
- Mottram, JT. 1992.** Lateral-torsional buckling of thin-walled composite I-beams by the finite difference method. *Composites Engineering*, 2(2): 91-104. doi: 10.1016/0961-9526(92)90048-B.
- Naderian, HR., Ronagh, HR. 2015.** Buckling analysis of thin-walled cold-formed steel structural members using complex finite strip method. *Thin-Walled Structures*, 90:74-83. doi:10.1016/j.tws.2015.01.008.
- Osman, HS., Ozkan, I., Erkmen, R. 2024.** Buckling analysis of thin-walled I-beams with web deformations. *Structures*, 69:107498. doi:10.1016/j.istruc.2024.107498.
- Palermo, L., Rachid, M., Venturini, WS. 1992.** Analysis of thin walled structures using the boundary element method. *Engineering Analysis with Boundary Elements*, 9(4):359-363. doi: 10.1016/0955-7997(92)90021-X.
- Pavazza, R., Matoković, A., Vukasović, M. 2022.** A theory of torsion of thin-walled beams of arbitrary open sections with influence of shear. *Mechanics Based Design of Structures and Machines*, 50(1): 206-241. doi:10.1080/15397734.2020.1714449.
- Prokić, A. 1994.** Material Nonlinear Analysis of Thin-Walled Beams. *Journal of Structural Engineering*, 120(10):2840-2852. doi: 10.1061/(ASCE)0733-9445(1994)120:10(2840).
- Prokić, A. 1996a.** New Warping Function for Thin-Walled Beams. I: Theory. *Journal of Structural Engineering*, 122(12):1437-1442. doi:10.1061/(ASCE)0733-9445(1996)122:12(1437).
- Prokić, A. 1996b.** New Warping Function for Thin-Walled Beams. II: Finite Element Method and Applications. *Journal of Structural Engineering*, 122(12):1443-1452. doi: 10.1061/(ASCE)0733-9445(1996)122:12(1443).
- Reddy, JN. 2004.** *Mechanics of Laminated Composite Plates and Shells: Theory and Analysis*. CRC Press.
- Sheikh, AH., Thomsen, OT. 2008.** An efficient beam element for the analysis of laminated composite beams of thin-walled open and closed cross sections. *Composites Science and Technology*, 68(10-11): 2273-2281. doi:10.1016/j.compsci-tech.2008.04.018.
- Shen, Z. 2024.** Thin-walled composite beam elements via the absolute nodal coordinate formulation. *Multibody System Dynamics*, 62:107-135. Doi:10.1007/s11044-023-09956-y.
- Soltani, M., Asgarian, B. 2018.** Determination of Lateral-Torsional Buckling Load of Simply Supported Prismatic Thin-Walled Beams with Mono-Symmetric Cross-Sections Using the Finite Difference Method. *Amirkabir Journal of Civil Engineering*, 50(1):23-26. doi: 10.22060/ceej.2017.11194.4986.
- Stoykov, S., Manoach, E., Margenov, S. 2016.** An efficient 3D numerical beam model based on cross sectional analysis and Ritz approximations. *Journal of Applied Mathematics and Mechanics*, 96(7): 791-812. doi:10.1002/zamm.201400139.
- Van Erp, G., Menken, C. 1990.** The spline finite-strip method in the buckling analyses of thin-walled structures *Communications in Applied Numerical Methods*, 6(6): 477-484. doi: 10.1002/cnm.1630060608.
- Vieira, RF., Virtuoso, FB., Pereira, EBR. 2014.** A higher order model for thin-walled structures with deformable cross-sections. *International Journal of Solids and Structures*, 51(3-4): 575-598. doi:10.1016/j.ijsolstr.2013.10.023.
- Vlasov, VZ. 1961.** *Thin-Walled Elastic Beams*, Second edition, Israel program for scientific translations, Jerusalem.
- Vo, TP., Lee, J. 2008.** Flexural-torsional behavior of thin-walled composite box beams using shear-deformable beam theory. *Engineering Structures*, 30(7): 1958-1968. doi:10.1016/j.engstruct.2007.12.003.
- Vo, TP., Lee, J. 2009.** Flexural-torsional behavior of thin-walled composite space frames. *International Journal of Mechanical Sciences*, 51(11-12):837-845. doi:10.1016/j.ijmecsci.2009.09.019.
- Vojnić-Purčar, M., Prokić, A., Bešević, M. 2019.** A numerical model for laminated composite thin-walled members with openings considering shear lag effect. *Engineering Structures*, 185: 392-399. doi:10.1016/j.engstruct.2019.01.142.
- Vukasović, M., Pavazza, R., Vlák, F. 2017.** Analytic solution for torsion of thin-walled laminated composite beams of symmetrical open cross sections with influence of shear. *The Journal of Strain Analysis for Engineering Design*, 52(3): 190-203. doi:10.1177/0309324717697524.

- Wang, XF., Yang, QS., Law S-S. 2014.** A shear locking-free spatial beam element with general thin-walled closed cross-section. *Engineering Structures*, 58:12–24. doi:10.1016/j.engstruct.2013.09.046.
- Yanlin, G., Shaofan, C. 1991.** Postbuckling interaction analysis of cold-formed thin-walled channel sections by finite strip method. *Thin-Walled Structures*, 11(3): 277-289. doi:10.1016/0263-8231(91)90004-3.
- Yu, W., Hodges, D.H., Ho, J.C. 2012.** Variational asymptotic beam sectional analysis - An updated version. *International Journal of Engineering Science*, 59: 40-64. doi:10.1016/j.ijengsci.2012.03.006.
- Zhang, YM., Gu, Y., Chen, JT. 2011.** Boundary element analysis of 2D thin walled structures with high-order geometry elements using transformation. *Engineering Analysis with Boundary Elements*, 35(3):581-586. doi:10.1016/j.enganabound.2010.07.008.